

# Impacts of the Imidazolate Linker Substitution (CH<sub>3</sub>, Cl, or Br) on the Structural and Adsorptive Properties of ZIF-8

Gérald Chaplais,<sup>\*,†,‡,§</sup> Guillaume Fraux,<sup>§</sup> Jean-Louis Paillaud,<sup>†,‡</sup> Claire Marichal,<sup>†,‡</sup> Habiba Nouali,<sup>†,‡</sup> Alain H. Fuchs,<sup>§</sup> François-Xavier Coudert,<sup>§</sup> and Joël Patarin<sup>†,‡,§</sup>

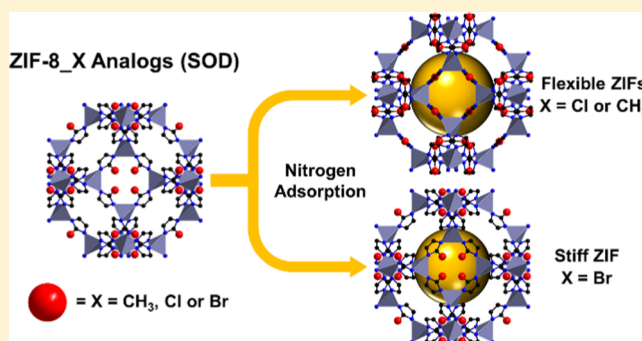
<sup>†</sup>Université de Haute-Alsace, CNRS, Axe Matériaux à Porosité Contrôlée (MPC), Institut de Science des Matériaux de Mulhouse (IS2M), UMR 7361, F-68100 Mulhouse, France

<sup>‡</sup>Université de Strasbourg, France

<sup>§</sup>Chimie ParisTech, PSL University, CNRS, Institut de Recherche de Chimie Paris, 75005 Paris, France

## Supporting Information

**ABSTRACT:** Zeolitic Imidazolate Frameworks (ZIFs) represent a thriving subclass of metal–organic frameworks (MOFs) owing to the large variety of their topologies, of which some of them are common with zeolites, and the ability to modulate the chemistry of their frameworks as well as the hydrophobicity/hydrophilicity balance, making them perfect examples of the isorecticular chemistry concept. One peculiar structural feature of ZIFs is their potential for structural transitions by rotation (or swing) of their linkers under external stimuli (guest adsorption, mechanical constraints, etc.). This singular characteristic, often denominated “swing effect” or “gate opening”, is related to flexible ZIFs. Our study focuses on the influence of the functional group (–CH<sub>3</sub>, –Cl, –Br) borne in position 2 by the imidazolate linker on the flexible/stiff nature of three isorecticular ZIFs with SOD topology. In the first part, we report the structures of ZIF-8\_Cl and ZIF-8\_Br, two halogenated analogs of the well-known ZIF-8 (herein named ZIF-8\_CH<sub>3</sub>), thanks to synergistic contributions of powder X-ray diffraction and <sup>13</sup>C MAS NMR spectroscopy. In both cases, a disorder of the linker is noted and characterized by two quasi-equal occupancies of the two linker subsets in the asymmetric unit. Experimental nitrogen sorption measurements, performed at 77 K for the three isorecticular ZIFs, combined with first-principles molecular dynamics simulations bring to light the flexibility of ZIF-8\_CH<sub>3</sub> and ZIF-8\_Cl and the stiffness of ZIF-8\_Br.



## INTRODUCTION

Zeolitic Imidazolate Frameworks (ZIFs) constitute a subclass of metal–organic frameworks (MOFs) and represent an emerging family of microporous materials owing to their chemical and thermal stabilities as well as textural properties (microporous volume and surface areas) compared to a large number of MOFs.<sup>1–4</sup> ZIFs are mainly built from divalent metal ions (e.g., Zn<sup>2+</sup>, Co<sup>2+</sup>, Cd<sup>2+</sup>, Cu<sup>2+</sup>) bridged by ditopic imidazolate-type anionic linkers. Each metal cation is most often tetrahedrally linked, through nitrogen atoms, to four imidazolate linkers, thereby leading essentially to extended three-dimensional structures.<sup>1,5–7</sup>

Thanks to their intrinsic physicochemical features, a vast field of applications involving ZIFs, such as, for example, gas storage,<sup>5,8–10</sup> separation,<sup>3,7,11–16</sup> encapsulation,<sup>3,17</sup> and catalysis,<sup>18–20</sup> has been explored. In the last few years, we have developed a new type of application, that is, energetic applications involving such materials from both experimental and modeling approaches.<sup>21–28</sup>

In a recent study,<sup>27</sup> some of the authors compared the energetic performance using high-pressure intrusion–extrusion experiments of nonwetting liquids (water, KCl, and LiCl aqueous solutions) in three sodalite (SOD) ZIF-8 derivatives, herein named ZIF-8\_CH<sub>3</sub> (commonly known as ZIF-8), ZIF-8\_Cl, and ZIF-8\_Br. The latter are two analogs of ZIF-8\_CH<sub>3</sub> with chlorine or bromine atoms borne in position 2 by the linker instead of methyl group. Significant differences in terms of energetic behaviors concerning the nine studied “ZIFs–nonwetting liquids” systems have encouraged us to further analyze the considered materials, especially ZIF-8\_Cl and ZIF-8\_Br, by examining their crystallographic structures and evaluating their potential flexibility.

These two halogenated hybrids were reported for the first time by Li et al.<sup>29,30</sup> for the assessment of their kinetic separation properties of propane/propene. Even if the authors listed the

Received: September 6, 2018

Revised: October 30, 2018

Published: October 30, 2018

related crystal data and structure refinement parameters and deposited the information in the Cambridge Structural Database,<sup>31</sup> referenced as AWIWEJ and AWIWIN, actually for only the crude compounds, namely, the hybrid matrixes with the remaining occluded solvent molecules, no further details about the needed atomic positions were provided from the two sources. Later, solely ZIF-8\_Cl (also named ZIF-Cl) was investigated in relation to isostructural ZIFs as part of CO<sub>2</sub> capture/separation by using density functional theory calculations<sup>32</sup> and Grand Canonical Monte Carlo (GCMC) simulations<sup>33</sup> or to estimate their hydrophobic/hydrophilic nature by combining molecular simulation results with a quantitative structure–property relationship.<sup>34</sup>

On another note, one distinctive property of some of the ZIFs lies in the possibility of structural transitions, occurring through rotation (or swing) of the linkers, which highlights the flexibility of these materials. For ZIF-8\_CH<sub>3</sub>, this was evidenced by the structural work of Moggach et al.,<sup>35</sup> which has shown that the swing of linkers occurs upon high pressure in diamond anvil cell high-pressure experiments. Fairen-Jimenez et al. evidenced also this peculiar phenomenon through a combined experimental-simulation study based on nitrogen sorption measurements and crystallographic results.<sup>36</sup> They assigned a step observed at low relative pressure in the isotherm to the structural transition. Ania et al. used experimental and simulation studies in order to demonstrate that this reorientation is governed by characteristics (polarizability, molecular size, shape) of the investigated gases (N<sub>2</sub>, Ar, O<sub>2</sub>, CO) and that the stepped adsorption behavior is defined by the guest packing inside the host.<sup>37</sup> Afterward, several investigations shed light on the correlation between the crystal size/shape of ZIF-8\_CH<sub>3</sub> and the stepped uptake profile noticed at low relative pressure in the nitrogen/argon sorption isotherms, thereby underlining the possibility to modulate the triggering of the swing of linkers.<sup>38–41</sup> Besides, the flexibility of ZIF-8\_CH<sub>3</sub> has also been characterized by using <sup>129</sup>Xe NMR spectroscopy.<sup>42</sup> Finally, it was recently shown by a combination of quantum chemistry calculations and first-principles molecular dynamics (MD) simulations that the structural transition featured upon adsorption for ZIF-8\_CH<sub>3</sub> is continuous as the function of pore loading and that thermodynamics of packing effects contribute to explain the experimental stepped adsorption isotherms.<sup>43</sup>

Consequently, volumetric nitrogen sorption and molecular dynamics (MD) simulations constitute complementary and suitable tools in order to appreciate the flexible/stiff behavior of ZIFs. Herein, we report firstly a full crystallographic study of ZIF-8\_Cl and ZIF-8\_Br based on a synergetic combination of powder X-ray diffraction (PXRD) and <sup>13</sup>C MAS NMR spectroscopy techniques. In a second part, we discuss in details about the nitrogen sorption isotherms of ZIF-8\_Cl and ZIF-8\_Br compared to the one of ZIF-8\_CH<sub>3</sub> performed at 77 K before commenting on the related results provided by molecular dynamic simulations.

## ■ EXPERIMENTAL SECTION

**Materials. Reagents and Solvents.** The reagents, zinc nitrate hexahydrate (Zn(NO<sub>3</sub>)<sub>2</sub>·6H<sub>2</sub>O, 99%), 2-methylimidazole (Hmim, 97%), 2-chloroimidazole (Hcim-2, 97%), and 2-bromoimidazole (Hbim-2, 95%), were provided by Alfa Aesar. The alcoholic solvents such as methanol (MeOH, 99.9%) and ethanol (EtOH, 99.9%) were purchased from Carlo Erba, whereas the basic ammonium hydroxide solution (NH<sub>3</sub>, 31.5%) was supplied by Sigma-Aldrich. Homemade deionized water was

also used to prepare ZIF-8\_CH<sub>3</sub>. All the reagents, base, and solvents were used without further purifications.

**Synthesis of ZIF-8\_CH<sub>3</sub>.** The synthesis protocol of He et al.<sup>44</sup> was followed with modifications in terms of quantities (ca. 12 times upscaling), recovering of material (filtration instead of centrifugation), and activation (soakings in MeOH) processes. Briefly, in a glass bottle, 7.01 g (23.6 mmol) of Zn(NO<sub>3</sub>)<sub>2</sub>·6H<sub>2</sub>O are dissolved under stirring in 39.00 g (2164.3 mmol) of deionized water to form a solution (S<sub>1</sub>). Meanwhile, in a 250 mL round bottom flask, 3.87 g (47.1 mmol) of Hmim are dissolved under stirring in 40.78 g (754.3 mmol NH<sub>3</sub>) of aqueous ammonia to get a solution (S<sub>2</sub>). Afterward, S<sub>1</sub> is added to S<sub>2</sub> under stirring. The final composition in molar equivalents of the reaction mixture is 1 Zn / 2 Hmim / 32 NH<sub>3</sub> / 164 H<sub>2</sub>O. After 10 min of stirring, a white suspension is obtained. A white solid is recovered by filtration and washed abundantly (420 mL) with deionized water per portion in order to lower the pH of the filtrate at around 7. After drying under air overnight, the white solid is soaked in 100 mL of MeOH for 4 h and recovered by filtration. The activation stage is repeated three times more. After drying under air, 1.79 g of white powder is obtained (yield of 33%). Powder X-ray diffraction (not shown) and thermogravimetric analysis (see Figure S1) evidenced the crystalline purity of the sample and the absence of occluded molecules.

**Synthesis of ZIF-8\_Cl.** The synthesis protocol was adapted from the one provided by Li et al.<sup>29</sup> by changing the quantities (ca. 11 times upscaling based on Zn source), the nature of the solvent (EtOH instead of MeOH), the linker on metal source ratio (2.0 instead of 2.6) as well as the composition in molar equivalents, and the heating duration (3 instead of 2 days). In a 150 mL poly(tetrafluoroethylene)-lined stainless steel autoclave, 1.37 g (4.6 mmol) of Zn(NO<sub>3</sub>)<sub>2</sub>·6H<sub>2</sub>O is dissolved in 74.00 g (1606.3 mmol) under stirring. Afterward, 0.98 g (9.2 mmol) of Hcim-2 is added, thereby resulting for the reaction mixture the following molar composition in equivalents: 1.0 Zn / 2.0 Hcim-2 / 350 EtOH / 6 H<sub>2</sub>O. After a 10 min stirring, the suspension is heated at 100 °C for 72 h. After cooling down to room temperature, 0.90 g of an ecru powder is obtained (yield of 73%) after filtration, washing with 100 mL of EtOH and drying at 70 °C for 3 h. Powder X-ray diffraction (see Figure S2) and thermogravimetric analysis (see Figure S1) proved the crystalline purity of the sample and the absence of occluded molecules.

**Synthesis of ZIF-8\_Br.** The synthesis protocol was also adapted from the one provided by Li et al.<sup>29</sup> where the quantities were increased (ca. 11 times upscaling based on Zn source, with 1.36 g (4.6 mmol) of Zn(NO<sub>3</sub>)<sub>2</sub>·6H<sub>2</sub>O) and synthesis stages (molar composition in equivalents of reaction mixture, container type, heating temperature, and duration, as well as washing process) were the same ones as previously followed for ZIF-8\_Cl except that Hcim-2 was substituted with Hbim-2. Then, 1.24 g of an ecru powder is obtained (yield of 75%). Powder X-ray diffraction (see Figure S3) and thermogravimetric analysis (see Figure S1) highlighted the crystalline purity of the sample and the absence of occluded molecules.

**Characterization Techniques. Powder X-ray Diffraction.** A small amount of ZIF-8\_Br and ZIF-8\_Cl samples was transferred into glass capillaries (Mark-tube made of special glass, no. 14, outside diameter 0.3 mm, Hilgenberg GmbH) for powder XRD (PXRD) analysis. Two scans for each sample were collected between 6 and 95° (2θ) on a STOE STADI-P diffractometer in Debye–Scherrer geometry, equipped with a

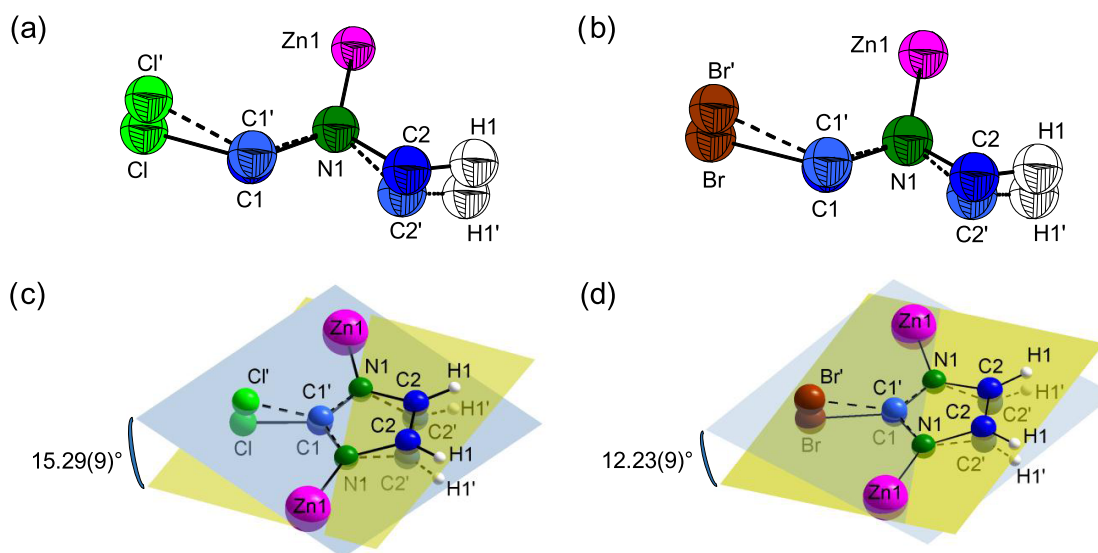


**Figure 1.** Asymmetric units of (a) ZIF-8\_Cl and (b) ZIF-8\_Br (50% of probability ellipsoid). Dihedral angles between the disordered imidazolate linkers of (c) ZIF-8\_Cl and (d) ZIF-8\_Br.

linear position-sensitive detector (PSD,  $6^\circ$  in  $2\theta$ ) and employing Ge monochromated Cu  $K_{\alpha 1}$  radiation ( $\lambda = 1.5406 \text{ \AA}$ ) (step  $0.01^\circ$ , 120 s of time acquisition per PSD step ( $0.1^\circ$ )). The two scans were averaged into a single one for better statistics on the collected data. The resulting powder X-ray diffraction patterns show well-resolved diffraction peaks, which confirm a good crystallinity. All diffraction peaks were ticked and indexed with the WinX<sup>POW</sup> package<sup>45</sup> using the Louër algorithm<sup>46</sup> with a cubic unit cell and refined in space group  $\bar{1}43m$  (no. 217) with  $a = 17.0370(3) \text{ \AA}$  (FOM(30) = 548.5) and  $a = 17.0832(6) \text{ \AA}$  (FOM(30) = 709.2) for ZIF-8\_Cl and ZIF-8\_Br, respectively. The Rietveld analysis<sup>47</sup> was performed with the GSAS package<sup>48</sup> and EXPGUI as an interface.<sup>49</sup> A Le Bail refinement<sup>50</sup> enabled the determination of the background and profile parameters. The empty structure of ZIF-8\_CH<sub>3</sub> described in space group  $\bar{1}43m$  and published by Moggach et al. (CCDC 739168 and RefCode TUDKEJ),<sup>35</sup> where the CH<sub>3</sub> group in position 2 of the linker was here replaced by a Cl or Br atom, was used as the starting model for the Rietveld refinement. After the first stage of the Rietveld analysis, after scale factor determination, Fourier difference maps showed unambiguously for both compounds a splitting of the halogen atomic positions on both sides of the imidazolate plane. This splitting is explained by a tilt of the linker around the axis defined by both nitrogen atoms. Following this observation and to take this disorder into account, a second set of atoms defining a differently oriented linker was introduced with the same shared nitrogen atoms. Each moiety having a specific occupancy factor, the sum of them was constrained to one. During the Rietveld refinement process, all atoms were refined isotropically, and soft restraints (bonds, angles, and planes) were added to maintain a proper structure of the imidazolate linker. The final Rietveld refinement gave excellent reliability factors; crystal as well as Rietveld refinement parameters are listed in Tables S1 and S4. Atomic parameters and selected bond distances and angles are listed in Tables S2, S3, S5, and S6. Crystallographic information files (CIF files) of ZIF-8\_Cl and ZIF-8\_Br can be obtained from the Cambridge Crystallographic Data Centre, quoting deposition numbers CCDC 1860457 and 1860456, respectively.

<sup>13</sup>C MAS NMR Spectroscopy. <sup>1</sup>H decoupled <sup>13</sup>C solid-state MAS NMR spectra were recorded on a Bruker AVANCE II 400WB spectrometer ( $B_0 = 9.4 \text{ T}$ ) operating at 100.64 MHz for <sup>13</sup>C and 400.18 MHz for <sup>1</sup>H. Samples were packed in a 4 mm cylindrical zirconia rotor and spun at a spinning frequency of 12 kHz. Experiments were performed with a  $\pi/4$  pulse duration of 2.7  $\mu\text{s}$  and a recycle delay of 60 s. <sup>13</sup>C chemical shifts were referenced to tetramethylsilane. Decomposition of the NMR spectra to extract the proportion of the corresponding species was performed with DMfit software.<sup>51</sup>

**Nitrogen Adsorption–Desorption Measurements.** Nitrogen adsorption–desorption isotherms were performed at 77 K using a Micromeritics ASAP 2420 apparatus. Prior to performing the sorption measurements, the samples were outgassed at 473 K for 12 h under secondary vacuum. The Langmuir and Brunauer–Emmett–Teller surface areas, denoted  $S_L$  and  $S_{\text{BET}}$ , respectively, were calculated according to the criteria specified in the literature<sup>52,53</sup> by applying thereby the corresponding models to the  $0.0004 \leq p/p^\circ \leq 0.0034$  range for ZIF-8\_CH<sub>3</sub>, in the  $0.0003 \leq p/p^\circ \leq 0.0047$  range for ZIF-8\_Cl, and in the  $0.0001 \leq p/p^\circ \leq 0.0018$  range for ZIF-8\_Br. The microporous volumes, named  $V_{\mu\text{p}}$ , were determined according to the  $t$ -plot method (Harkins and Jura model) for a thickness of 6–12  $\text{\AA}$  for ZIF-8\_CH<sub>3</sub> and ZIF-8\_Br and 10–16  $\text{\AA}$  for ZIF-8\_Cl. Accessible volumes for the three ZIF-8 derivatives are mapped in Figure S4, and Supporting Information are summed up in Table S7.

**Scanning Electron Microscopy.** The size and shape of the ZIF-8 derivatives crystals were determined by scanning electron microscopy using a Philips XL 30 FEG microscope. The micrographs are supplied in Figure S5.

**Molecular Simulation Methods.** To probe the relationship between the structure changes and the adsorbed molecules, we used molecular dynamics (MD) simulations. To describe fully the flexibility of the frameworks without any assumption, we favored first-principles molecular dynamics (also called *ab initio* molecular dynamics) over force field-based MD—as there are currently no force fields available for the various ZIF-8 variants studied here. For each framework (ZIF-8\_CH<sub>3</sub>, ZIF-8\_Cl, ZIF-8\_Br), we ran five simulations corresponding to different number  $N$  of nitrogen molecules inside the porous space, going

from empty framework ( $N = 0$ ) to the fully loaded host material. The maximal loading was determined from the experimental isotherms to be close to  $N = 50$  molecules per unit cell for ZIF-8\_CH<sub>3</sub> and ZIF-8\_Cl and  $N = 40$  molecules per unit cell for ZIF-8\_Br. To create the starting configurations, we started from the energy-minimized configuration of the empty frameworks and randomly placed the selected number of nitrogen molecules in the unit cell. The whole {ZIF, adsorbate} system was then minimized again before starting the molecular dynamics simulations.

We used the Quickstep module<sup>54</sup> of the CP2K software package (version 2.5.1, available online at <http://www.cp2k.org/>) for all the simulations, with a Perdew–Burke–Ernzerhof exchange–correlation functional<sup>55</sup> with D3 dispersion corrections,<sup>56</sup> a double zeta polarizable valence basis set, and an energetic cutoff of 600 Ry. All the systems were simulated with a 1 fs time step, giving a total of 12–22 ps of simulation. Temperature was held constant at 77 K with a CVSR thermostat,<sup>57</sup> using a thermostat time constant of 1000 fs. We used the last 5 ps of simulation for analysis, leaving time to the system to equilibrate. Representative input files for the molecular dynamics simulations are available online in the data repository at <https://github.com/fxcoudert/citable-data>.

## RESULTS AND DISCUSSION

### Structural Characterizations of ZIF-8\_Cl and ZIF-8\_Br.

**Structure Description of ZIF-8\_Cl and ZIF-8\_Br.** The structural study from Rietveld analysis reveals a similar disorder for both structures. It is highlighted in Figure 1a,b representing the asymmetric units of ZIF-8\_Cl and ZIF-8\_Br and where an occupancy factor of approximately 50% for the tilted linkers was refined in both cases (see Tables S2 and S5). In Figure 1c, the dihedral angles between the disordered halogenated imidazolate planes are slightly greater for ZIF-8\_Cl in comparison with the one observed for ZIF-8\_Br (see Figure 1d), the difference being of about 3°.

Such a disorder in ZIF of topology SOD exists in SALEM-2, which has been synthesized via a partial solvent-assisted linker exchange (SALE) of 2-methylimidazolate by imidazolate from the nondisordered ZIF-8\_CH<sub>3</sub>.<sup>58</sup> Besides, Springer et al. have recently demonstrated from theory and experiment that Zn-based ZIFs of SOD topology prepared with 4,5-dichlorinated imidazolate linkers are subject to different orders and/or disorders having distinctly different linker orientations with small energy differences.<sup>59</sup> On the other hand, in the same study, they concluded that such disorder cannot exist in SOD-type ZIFs with 2-substituted imidazolate linkers. The present study tends to prove the opposite.

For ZIF-8\_Br and ZIF-8\_Cl, the linker disorder involves also two different dihedral angles between the plane defined by the six zinc atoms of the six-membered ring of the sodalite cage and the linker plane;<sup>43</sup> they are of 3.60(7) and 11.69(6)° for ZIF-8\_Cl and 0.61(7) and 11.62(6)° for ZIF-8\_Br. These values are consistent with the computed distributions in the case of zero adsorbed N<sub>2</sub> molecule even if only one configuration is taken into account for the calculation (see Computational Study).

**<sup>13</sup>C NMR MAS Measurements.** <sup>13</sup>C MAS NMR is a powerful tool to probe the local environment of carbon atoms belonging to the framework linkers of ZIFs and gives complementary information to powder XRD results, making possible a reliable structure elucidation. Figure 2 displays the <sup>1</sup>H decoupled <sup>13</sup>C MAS NMR spectra of the three samples. The spectrum of ZIF-8\_CH<sub>3</sub> presents three resonances (as expected from the

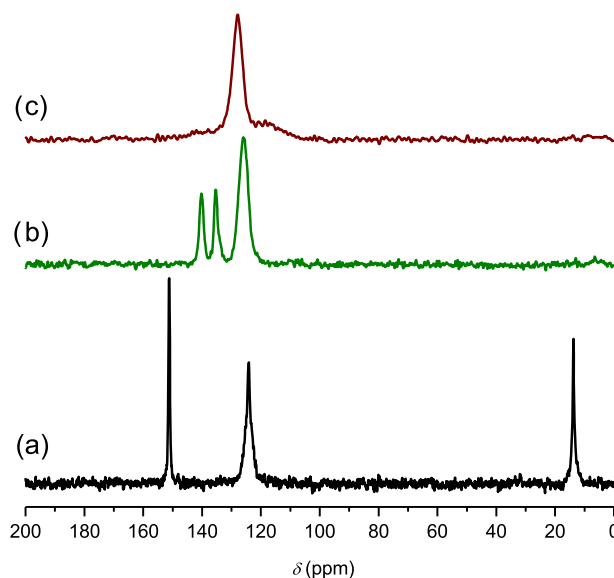


**Figure 2.** <sup>1</sup>H decoupled <sup>13</sup>C MAS NMR spectra of (a) ZIF-8\_CH<sub>3</sub>, (b) ZIF-8\_Cl, and (c) ZIF-8\_Br.

asymmetric unit<sup>36</sup>) at 13.8, 124.2, and 151.2 ppm accounting for 26, 48, and 26% of the total signal, respectively. These resonances are assigned to the methyl group, the two protonated aromatic carbon atoms, and the quaternary carbon atom of the 2-methylimidazolate (mim) linker in agreement with the literature.<sup>60</sup> For ZIF-8\_Cl, two sharp resonances are detected at 140.2 and 135.4 ppm each accounting for 17% of the total signal, whereas a broader resonance is observed at 126 ppm corresponding to 66% of the signal. This latter resonance is assigned to the two protonated aromatic carbon atoms of the 2-chloroimidazolate (cim-2) linker. It is interesting to note that the width at midheight of this resonance is 375 Hz, that is, significantly greater than the one of the corresponding resonance in ZIF-8\_CH<sub>3</sub> (160 Hz). This is in agreement with the coexistence of two disordered linkers that are not resolved on the <sup>13</sup>C MAS NMR spectrum but probably responsible for the observed broadening. Moreover, the resonance corresponding to the quaternary carbon atom is split in two resonances of equal intensity in agreement with the suggested two different orientations of the cim-2 linker in the structure with 50% occurrence each. As expected, the substitution of the CH<sub>3</sub> group by a Cl atom shifts the resonance of the carbon atom bearing the substituent toward high field. For ZIF-8\_Br, a main component is detected at 127.9 ppm corresponding to the aromatic C–H. Despite a small deshielding of the resonance, the broadness is similar to the one observed for ZIF-8\_Cl. The resonance(s) corresponding to the quaternary carbon atom(s) is/are not resolved. Nevertheless, additional broad components around 140 and 120 ppm are observed that could account for the quaternary carbon atoms of the two different orientations of the 2-bromoimidazolate (bim-2) linker. Indeed, <sup>13</sup>C resonances corresponding to carbon atoms covalently bonded to quadrupolar nuclei such as <sup>79</sup>Br ( $I = 3/2$ ) can be broadened or split by second-order quadrupolar effects via residual dipolar coupling.<sup>61</sup> This effect is expected to be more significant for <sup>79</sup>Br than for <sup>35</sup>Cl ( $I = 3/2$ ) because the quadrupolar moment of <sup>79</sup>Br is 3.6 times greater than the one of <sup>35</sup>Cl.

**Flexibility or Stiffness of ZIF-8 Derivatives under Nitrogen Adsorption.** As already mentioned, the nitrogen sorption measurements, especially when they are combined with

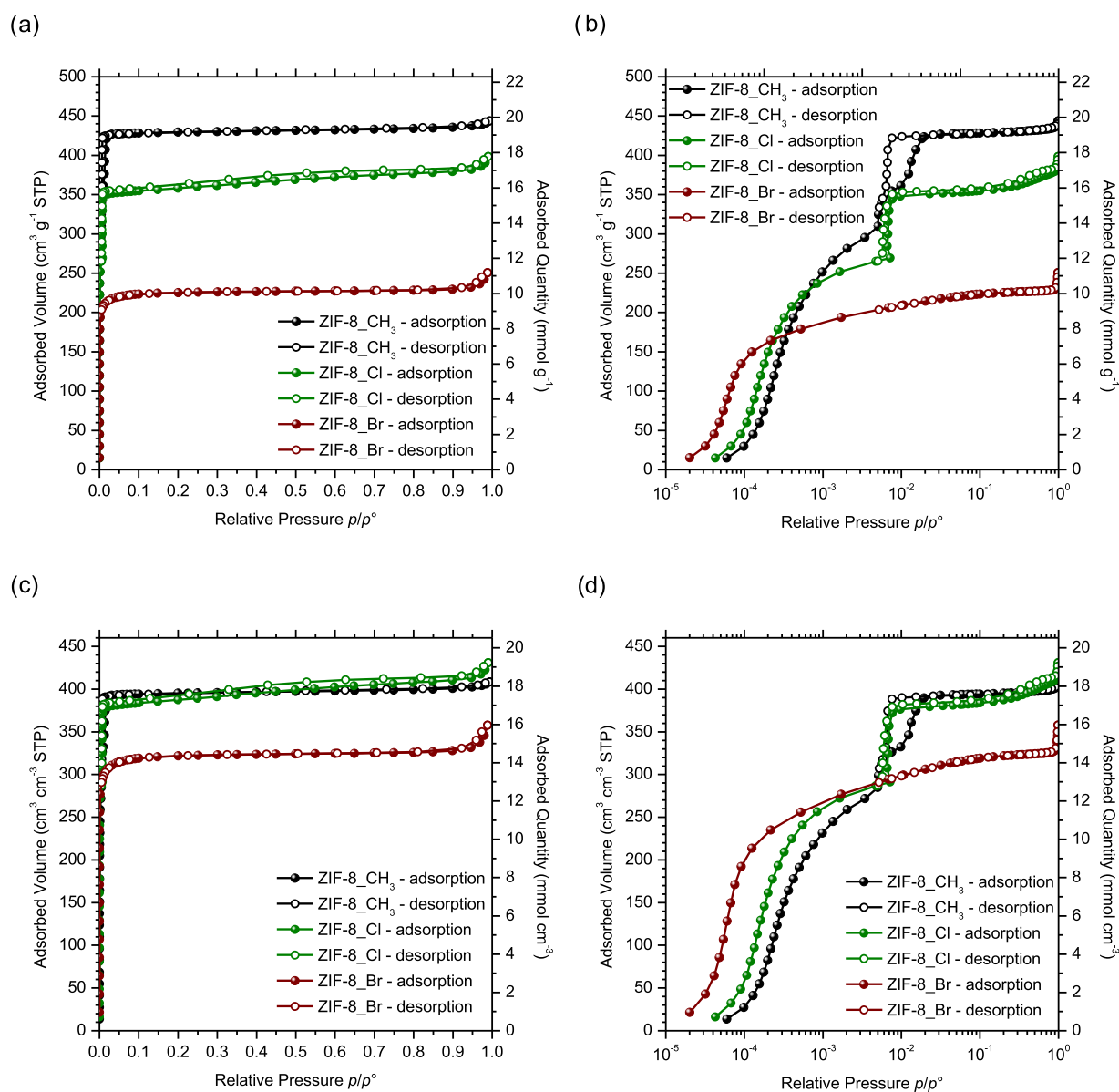


**Figure 3.** Nitrogen adsorption–desorption isotherms measured at 77 K of the ZIF-8 derivatives. Nitrogen uptakes are expressed (a, b) in  $\text{cm}^3 \text{g}^{-1}$  STP on the left axis and in  $\text{mmol g}^{-1}$  on the right axis, and (c, d) in  $\text{cm}^3 \text{cm}^{-3}$  STP on the left axis and in  $\text{mmol cm}^{-3}$  on the right axis. Plots are also given with (a), (c), a linear scale and (b), (d) a logarithmic scale of the relative pressure. Spherical and empty symbols correspond to the adsorption and desorption branches, respectively.

MD simulations, enable one to determine the flexible/stiff behavior of ZIF-type materials.

**Experimental Study.** The properties of the ZIF-8 derivatives were characterized by nitrogen adsorption–desorption measurements at 77 K. The corresponding isotherms are depicted in Figure 3a–d where the nitrogen sorption capacities are expressed as a function of the relative pressure and either in  $\text{cm}^3 \text{g}^{-1}$  STP and  $\text{mmol g}^{-1}$  (Figure 3a,b) or in  $\text{cm}^3 \text{cm}^{-3}$  STP and  $\text{mmol cm}^{-3}$  (Figure 3c,d). Figure 3b,d group the same plots as Figure 3a,c, respectively, but provided in the logarithmic instead of linear scale. The textural parameters are recapitulated in Table 1.

In more details, ZIF-8\_CH<sub>3</sub> isotherm is characterized by a two-stepped uptake starting at  $p/p^\circ \approx 0.005$  and ending at  $p/p^\circ \approx 0.02$  as well as by a sharper reverse phenomenon occurring in the 0.075–0.005  $p/p^\circ$  range. This leads to the formation of a hysteresis loop, which has been already shown dependent on the

**Table 1. Linker and Textural Parameters of ZIF-8 Derivatives<sup>a</sup>**

ZIF	ZIF-8_CH <sub>3</sub>	ZIF-8_Cl	ZIF-8_Br
linker	mim	cim-2	bim-2
$V_\mu$ ( $\text{cm}^3 \text{g}^{-1}$ )	0.66	0.57	0.35
$N_\mu$ (molecule per unit cell)	52.1	52.5	43.0
$S_{\text{BET}}$ ( $\text{m}^2 \text{g}^{-1}$ )	1380	1175	863
$S_L$ ( $\text{m}^2 \text{g}^{-1}$ )	1386	1181	865

<sup>a</sup>Microporous volume ( $V_\mu$ ), corresponding number of nitrogen molecules per unit cell ( $N_\mu$ ), BET ( $S_{\text{BET}}$ ), and Langmuir ( $S_L$ ) surface areas.

crystals' size and shape,<sup>38–41</sup> the nature of probe molecules, and the temperature of sorption measurements.<sup>37</sup> It reveals the flexibility of this material due to a structural transition based on the reorientation (swing) of linkers, making possible the

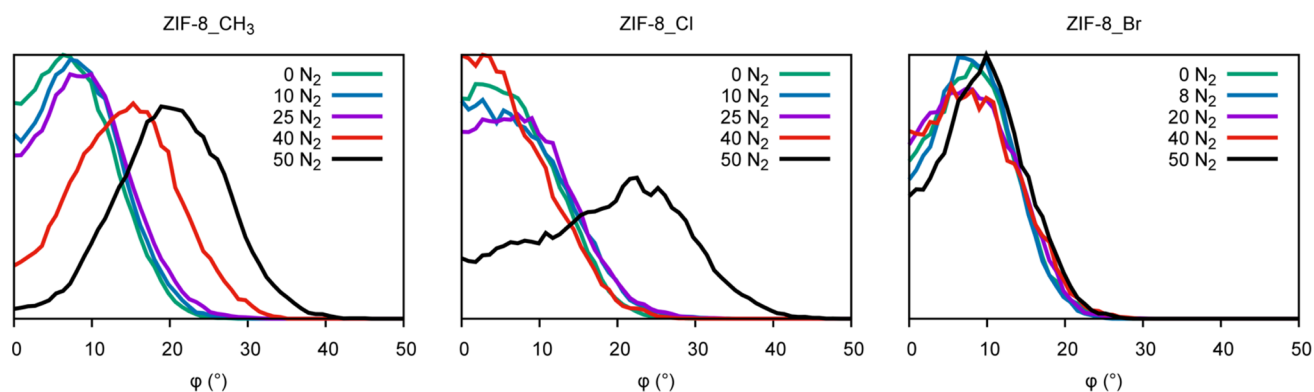


**Figure 4.** Distribution of linker swing angle  $\varphi$  (Zn–Zn–C–X dihedral angle, where X stands for CH<sub>3</sub>, Cl, or Br for ZIF-8\_CH<sub>3</sub>, ZIF-8\_Cl, or ZIF-8\_Br, respectively) at various values of nitrogen loading in ZIF-8\_CH<sub>3</sub>, ZIF-8\_Cl, and ZIF-8\_Br.

accommodation of large molecules<sup>62</sup> or more probe molecules than it is expected in the case of a stiff framework.<sup>36</sup> Indeed, the experimental microporous volume (0.66 cm<sup>3</sup> g<sup>-1</sup>), which is consistent with the literature,<sup>25</sup> exceeds ca. 25% of the theoretical value of 0.53 cm<sup>3</sup> g<sup>-1</sup> calculated for a stiff structure (see Table S7 and ref 63). A reversible uptake, taking place at low relative pressure ( $p/p^\circ \approx 0.007$ ), similar to ZIF-8\_CH<sub>3</sub>, is also noticed for ZIF-8\_Cl. Nevertheless, this phenomenon is labeled by a single-stepped and very sharp adsorption without hysteresis loop as the adsorption and desorption branches are superimposable. This is presumably due to the larger ZIF-8\_Cl crystals, which also tend to form agglomerates whose sizes reach several tens of micrometers, without presenting a specific shape (see Figure S5). In contrast, the ZIF-8\_CH<sub>3</sub> crystals display a well-defined chamfered cubic shape with a noticeable monodispersed size centered at ca. 600 nm. It is worthy to note that this sudden uptake observed for ZIF-8\_Cl enables the nitrogen capacity to increase significantly from 269.3 cm<sup>3</sup> g<sup>-1</sup> STP (or 0.42 cm<sup>3</sup> g<sup>-1</sup>, 12.0 mmol g<sup>-1</sup>, 291.2 cm<sup>3</sup> cm<sup>-3</sup> STP, 13.0 mmol cm<sup>-3</sup>, 38.7 molecules per unit cell) to 347.9 cm<sup>3</sup> g<sup>-1</sup> STP (or 0.54 cm<sup>3</sup> g<sup>-1</sup>, 15.5 mmol g<sup>-1</sup>, 376.3 cm<sup>3</sup> cm<sup>-3</sup> STP, 16.8 mmol cm<sup>-3</sup>, 50.0 molecules per unit cell) at  $p/p^\circ \approx 0.01$ . The swing of the *cim*-2 linkers in the SOD-type ZIF-8\_Cl structure, following the example of the one of *mim* linkers in ZIF-8\_CH<sub>3</sub>, explains why the latter surpasses the theoretical values evaluated at 0.47 (see Table S7) or 0.41 cm<sup>3</sup> g<sup>-1</sup>.<sup>32</sup> Furthermore, according to our computational study (see below), it is due to a repacking of nitrogen probe molecules inside the porous cages of ZIF-8\_Cl as pressure increases, enabling this material to fit more molecules inside the porous cavities. After a plateau between  $p/p^\circ \approx 0.01$  and 0.10, a second adsorption step, also reversible but much less marked than the previous one, is also noted for ZIF-8\_Cl. It occurs in the broad relative pressure range from 0.10 to 0.95 and thereby enhances more the nitrogen capacity, which totals 382.1 cm<sup>3</sup> g<sup>-1</sup> STP (or 0.59 cm<sup>3</sup> g<sup>-1</sup>, 17.0 mmol g<sup>-1</sup>, 413.2 cm<sup>3</sup> cm<sup>-3</sup> STP, 18.4 mmol cm<sup>-3</sup>, 54.9 molecules per unit cell) at the highest limit. Such an uptake at relative high pressure was already observed for ZIF-90 (with topology SOD and built from imidazolate-2-carboxyaldehyde) at  $p/p^\circ \approx 0.4$  but with a steeper effect. This was assigned to a slight constriction of the pores due to the presence of the aldehyde functionality on the linker,<sup>64</sup> a constriction in the pores,<sup>65</sup> or a gate-opening phenomenon.<sup>66</sup> For ZIF-8\_Cl, it remains still unclear whether this second step corresponds to slight modification of packing molecules or surface adsorption. However, our computational study (see below) suggests that it would be assigned to the

transition toward an accommodated molecules arrangement that is more ordered. It is also interesting to note a strong similarity between the isotherms of ZIF-8\_Cl and ZIF-8\_CH<sub>3</sub> (except for the second uptake) when the capacities are expressed in cm<sup>3</sup> cm<sup>-3</sup> (or in mmol cm<sup>-3</sup>) (see Figure 3c,d). For ZIF-8\_Br, the nitrogen physisorption measurements reveal a classical reversible type Ia isotherm.<sup>67</sup> The experimental microporous volume of 0.35 is consistent with the theoretical value of 0.32 cm<sup>3</sup> g<sup>-1</sup> (see Table S7). These experimental results, which are confirmed by the computational study (see below), evidence that ZIF-8\_Br constitutes a stiff porous material upon nitrogen adsorption and consequently that no reorientation (swing) of *bim*-2 linkers is observed presumably because of steric hindrance of Br atom borne in position 2 by the imidazolate. Moreover, the three functionalized ZIF-8 derivatives are also distinguishable by the sorption capacities at very low pressures, below  $p/p^\circ \approx 0.005$ –0.007, so before the “gate opening” pressures observed for ZIF-8\_CH<sub>3</sub> and ZIF-8\_Cl (see Figure 3b,d). The strength of interplays between nitrogen probe molecules and host materials frameworks decreases in the order: ZIF-8\_Br > ZIF-8\_Cl > ZIF-8\_CH<sub>3</sub>. The latter may be explained by electrostatic interactions or entropic parameters or a combination of both hypotheses. Indeed, even though the nitrogen molecules are commonly used for evaluating the textural properties of porous materials, they display a quadrupole moment<sup>68</sup> and may interact preferentially on the internal surface with linkers in the ascending order *mim* < *cim*-2 < *bim*-2 as all ZIFs are Zn-based materials. From a point of view concerning the entropy, the stiffness of ZIF-8\_Br structure could generate preferentially initial favorable adsorption sites in pore mouth for the 6-membered facets. Finally, Figure 3d, where nitrogen capacities of the ZIF-8 derivatives are expressed in cm<sup>3</sup> cm<sup>-3</sup> STP, highlights also a peculiar point resulting from the intersection of the three isotherms. This point takes place at  $p/p^\circ \approx 0.005$ –0.007 and corresponds to an adsorbed nitrogen capacity of ca. 13 mmol cm<sup>-3</sup> (ca. 38 molecules per unit cell). Above, from an experimental point of view, we have argued that this point represents the gate opening pressure due to the swing of linkers in the cases of ZIF-8\_CH<sub>3</sub> and ZIF-8\_Cl, thereby enabling more probe molecules to be accommodated. Given the high structural similitude of ZIF-8 counterparts (except the flexibility/stiff characteristic), the slight increase from 13 to 14.5 mmol cm<sup>-3</sup> observed for ZIF-8\_Br is certainly related to a slight modification packing of nitrogen molecules.

To provide insights into the mechanism behind the different behavior of the three frameworks with respect to nitrogen adsorption, a computational study was realized.

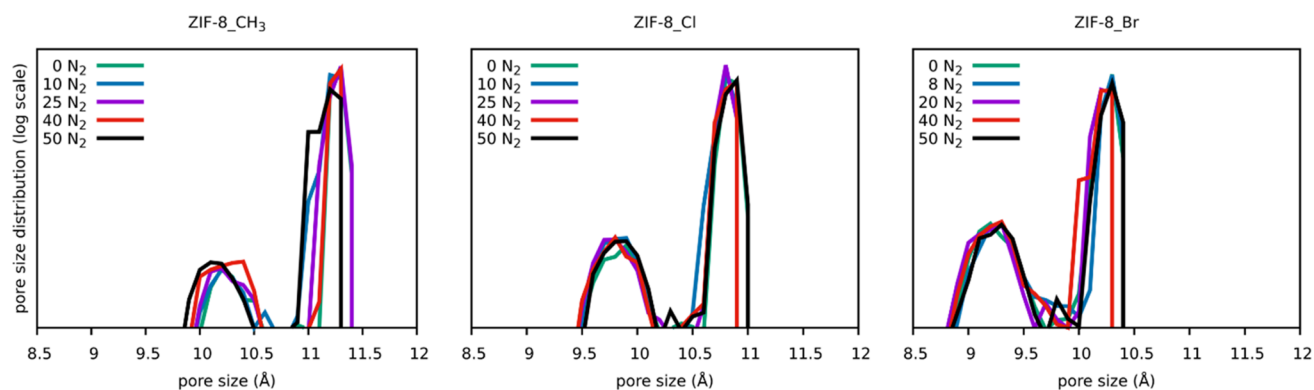


**Figure 5.** Pore size distribution (no unit) under increasing loading for the three structures.

**Computational Study.** The adsorption of nitrogen probe molecules at low temperature in parent compound ZIF-8 (herein named ZIF-8\_CH<sub>3</sub>) has already been studied extensively, both experimentally and by computational methods. Early work demonstrated that the structure of ZIF-8\_CH<sub>3</sub> goes through at least two phases during the adsorption: an ambient-pressure phase named AP (or ZIF-8 I) and a high-pressure phase named HP (or ZIF-8 II). These phases mainly differ by the orientation of the linkers around the 4- and 6-membered windows.<sup>36</sup> A recent, more detailed characterization of the structural evolution upon adsorption showed that the transition from AP to HP is linked to a continuous swing (rotation) of the mim linker, which can be followed as the dihedral angle Zn–Zn–C–CH<sub>3</sub> goes from an equilibrium value of 7° in the AP phase to an equilibrium value of 35° in the HP phase.<sup>43</sup>

In this work, the same approach using the Zn–Zn–C–X dihedral angle  $\varphi$  (where X stands for CH<sub>3</sub>, Cl, or Br for ZIF-8\_CH<sub>3</sub>, ZIF-8\_Cl, or ZIF-8\_Br, respectively) enabled us to follow the evolution of the three SOD frameworks upon nitrogen adsorption through first-principles molecular dynamics. The distributions of angles as a function of various nitrogen molecule loadings are shown in Figure 4 for the three ZIFs. For ZIF-8\_CH<sub>3</sub>, a gradual increase of the dihedral angle is observed versus the loading, while the distribution profile conserves a Gaussian type. These results are consistent with the already published ones for ZIF-8\_CH<sub>3</sub>. Interestingly, the two other frameworks behave differently. For ZIF-8\_Cl, no change is noticed in the distribution profile upon adsorption until the highest value of loading (i.e.,  $N = 50$ ). In this case, the distribution shifts and the profile are no longer Gaussian type. It indicates that some of the linkers do not rotate (swing) even at high loading. This nonzero value of the distribution at  $\varphi = 0$  contrasts with the case of ZIF-8\_CH<sub>3</sub>. Finally, for ZIF-8\_Br, no change occurs for the dihedral angle distribution as the loading increases.

Although correlated with it, this behavior is not however sufficient to explain the presence of the adsorption step encountered at low relative pressure ( $p/p^\circ \approx 0.005$ – $0.007$ ) in the nitrogen isotherms of ZIF-8\_CH<sub>3</sub> and ZIF-8\_Cl and its absence in the one of ZIF-8\_Br. One hypothesis often formulated for ZIF-8\_CH<sub>3</sub> is that the swinging motion leads to an increase of the accessible porous volume in the structure, thereby increasing nitrogen uptake. To show that this is not the case, and that the effect is more subtle, we computed the pore size distribution (PSD) (see Figure 5) and the accessible volume (see Figure 6) from our MD trajectories using Zeo++.<sup>69</sup> The results presented in Figure 5 highlight that the pore size

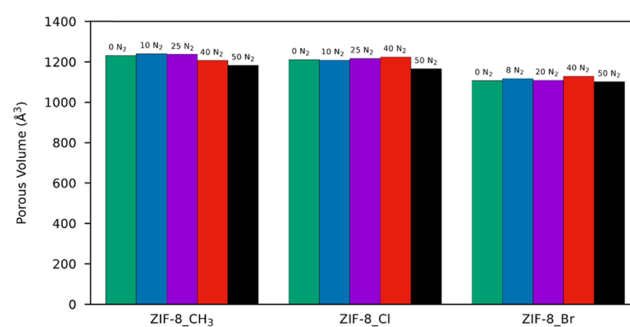


**Figure 6.** Porous volume changes in the three isorecticular structures during adsorption.

distribution (PSD) remains constant in all cases as the loading increases and the linkers swing. The three PSDs are similar albeit a shift toward smaller pores is noticeable in the order ZIF-8\_CH<sub>3</sub> > ZIF-8\_Cl > ZIF-8\_Br. This is also reflected in the accessible volume, which remains roughly constant as the loading increases and the linkers swing (see Figure 6).

The origin of the steep uptake at low relative pressure observed in the nitrogen sorption isotherm of ZIF-8\_CH<sub>3</sub> is actually linked to a reordering (repacking) of the nitrogen molecules in the cavity, thereby leading to an increase of adsorbed molecules in the same total pore volume as well as the swing of the linkers aiming to accommodate the new packing. This hypothesis had been already proposed by Ania et al., but the intermediate adsorption regime was then not probed or interpreted.<sup>37</sup> To visualize this packing, we have projected the positions of all adsorbed nitrogen atoms in the  $xy$  plane and created a density map of the adsorbed phase. Figure 7 groups the two-dimensional (2D) density maps of the positions of the adsorbed nitrogen atoms in the  $xy$  plane both at various loadings and for the three frameworks.

For ZIF-8\_CH<sub>3</sub>, two different molecular packings are encountered according to the loading. With 10 or 25 molecules in the unit cell, the density maps show clear delimited positions on a cubic-like arrangement, whereas with 40 and 50 molecules, they show a tetragonal-like arrangement of the molecules. This reordering of the adsorbed nitrogen molecules from a cubic-like phase to a tetragonal-like phase is at the origin of the steep uptake at low relative pressure. For ZIF-8\_Cl, the behavior is roughly similar: the molecules first pack in a cubic-like fashion in the cases of 10, 25, and 40 molecules per unit cell, before a reordering toward a tetragonal-like arrangement at 50 molecules per unit cell. This is consistent with the dihedral angle distributions as shown in Figure 4 and evidences that the

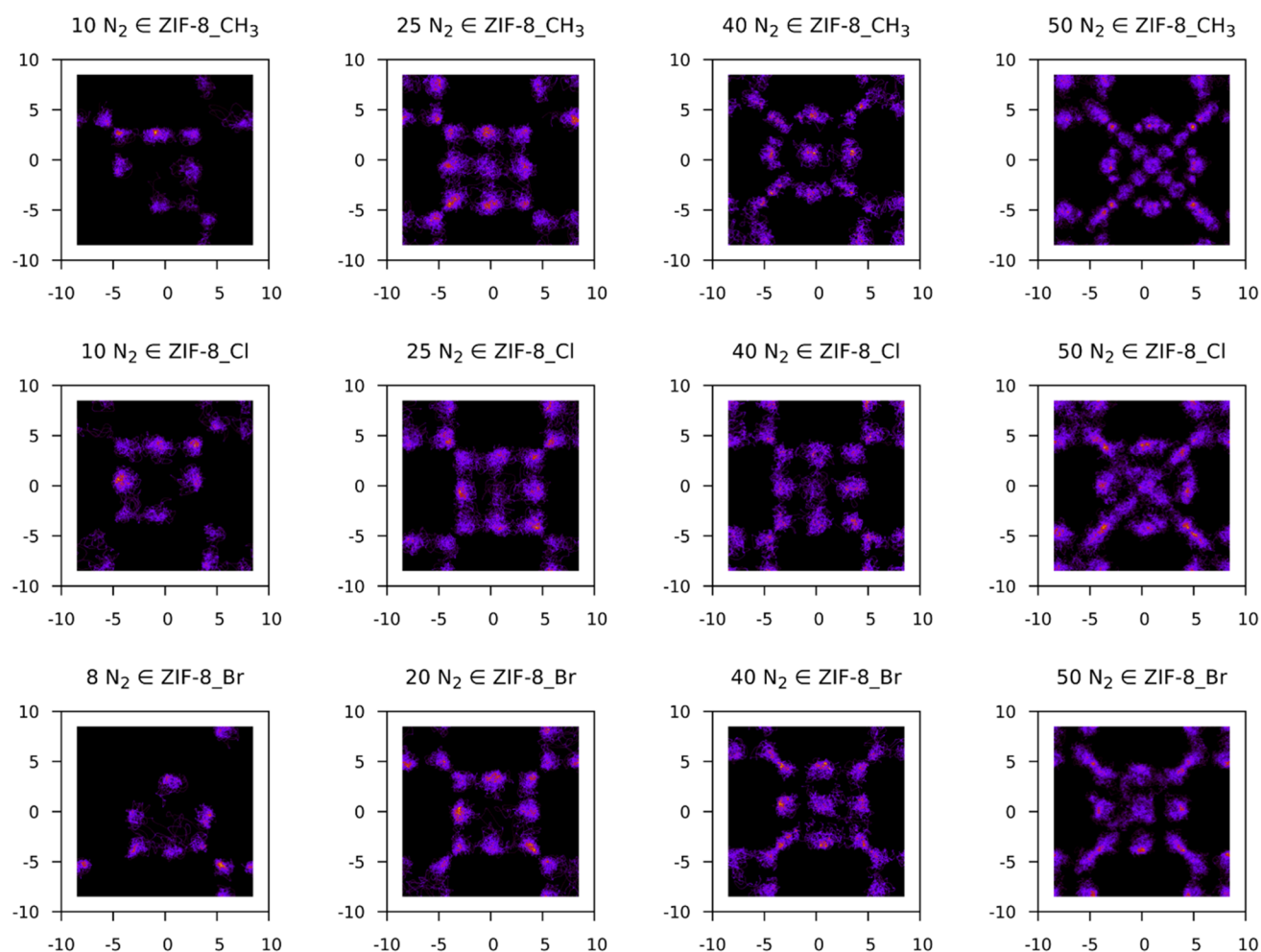


**Figure 7.** Two-dimensional (2D) density maps of the adsorbed nitrogen atom positions in the  $xy$  plane at various loadings in ZIF-8\_CH<sub>3</sub> (top), ZIF-8\_Cl (middle), and ZIF-8\_Br (bottom). The loading increases from left to right.

molecular packing rearrangement happens conjointly with the swing of the linkers. It is interesting to note that some disorder in the tetragonal arrangement remains for a loading of 50 molecules per unit cell as the molecule positions are not as well defined as the ones in ZIF-8\_CH<sub>3</sub>. Again, this is coherent with the dihedral angle distribution at 50 molecules per unit cell for ZIF-8\_Cl, which is not of a single Gaussian type, indicating that this disorder can also be found in the framework structure. For ZIF-8\_Br, the behavior is different. The same cubic-like arrangement is found at the lower loadings of 8 and 20 molecules per unit cell, whereas the arrangement at the higher loadings of 40 and 50 molecules per cell differs from the tetragonal-like one seen for ZIF-8\_CH<sub>3</sub> and ZIF-8\_Cl. Indeed, the latter appears as a mix of the cubic and the tetragonal organization as the molecules are mostly distributed on a cube with additional molecules in the [111] channels on the diagonals of the cube. Consequently, because of the absence of a neat reordering of adsorbed nitrogen molecules in ZIF-8\_Br, its sorption isotherm does not display the S-shaped adsorption step. Given that the change in functional group, and thus in partial atomic charges, does not significantly impact the strength of the Zn–N coordination bond, we ascribe the origin of this different sorption feature between the three ZIF-8 derivatives to the difference in pore size and shape, the pores in ZIF-8\_Br being too small to enable a molecular reordering to occur.

## CONCLUSIONS

Three ZIF-8 derivatives of SOD topology, that is, ZIF-8\_CH<sub>3</sub> (commonly known as ZIF-8), ZIF-8\_Cl (also called ZIF-Cl), and ZIF-8\_Br, have been prepared from imidazole-type organic sources functionalized in position 2 by a CH<sub>3</sub> group, Cl atom, or Br atom, respectively. The first part of this study is devoted to the description of the two structures (desolvated/activated phases) of the halogenated and isorecticular materials enabled by the contributions of powder X-ray diffraction and <sup>13</sup>C MAS NMR spectroscopy. These two techniques reveal a disorder (tilt) of the linker in the two investigated structures where the occupancy of the two subsets is about half. In the second part, the behaviors of the three MOFs under nitrogen molecules adsorption are comparatively screened. The experimental nitrogen sorption isotherms indicate that ZIF-8\_Cl behaves roughly as ZIF-8\_CH<sub>3</sub>, that is, with a singular, marked, and reversible uptake at low relative pressure. Conversely, ZIF-8\_Br displays a typical type Ia isotherm. These results show that ZIF-8\_Cl adopts a flexible structure like ZIF-8\_CH<sub>3</sub>, where a swing (rotation) of the linker makes the accommodation of 12–14 supplementary molecules per unit cell possible. By contrast, ZIF-8\_Br possesses a framework significantly more stiff. Furthermore, molecular dynamic simulations carried out on the three isorecticular structures corroborate these trends by evaluating the Zn–Zn–C–X dihedral angle (where X stands for CH<sub>3</sub>, Cl, or Br for ZIF-8\_CH<sub>3</sub>, ZIF-8\_Cl, or ZIF-8\_Br, respectively), which

evolves as a function of accommodated molecules for ZIF-8-CH<sub>3</sub> and ZIF-8-Cl but remains unchanged for ZIF-8-Br. Importantly, these simulation methods highlight that the structural transition (swing of linker) is triggered by a repacking of nitrogen molecules, thereby inducing this gate opening or “swing effect”. Finally, this study based on both experimental and simulation methods evidences clearly the influence of functional group borne by the linker on the flexible/stiff structural nature of three isorecticular ZIFs of SOD topology. A similar observation, involving ZIF-8-CH<sub>3</sub>, ZIF-90, and ZIF-65, with respective -CH<sub>3</sub>, -CH=O, and -NO<sub>2</sub> groups and using high-pressure single-crystal X-ray diffraction, density functional theory, and grand canonical Monte Carlo simulations, has been recently published.<sup>70</sup>

## ■ ASSOCIATED CONTENT

### Supporting Information

The Supporting Information is available free of charge on the ACS Publications website at DOI: 10.1021/acs.jpcc.8b08706.

TG curves of the three studied materials, crystallographic data of ZIF-8-Cl and ZIF-8-Br, assessment of nitrogen accessible volume for ZIF-8 derivatives, crystalline morphologies of ZIF-8 derivatives (PDF)

## ■ AUTHOR INFORMATION

### Corresponding Author

\*E-mail: gerald.chaplais@uha.fr. Tel: +33 389 33 68 87.

### ORCID

Gérald Chaplais: 0000-0003-2756-4896

François-Xavier Coudert: 0000-0001-5318-3910

Joël Patarin: 0000-0002-6511-5357

### Funding

We acknowledge access to the CINES high-performance computing platforms provided by GENCI grant A0030807069.

### Notes

The authors declare no competing financial interest.

## ■ ACKNOWLEDGMENTS

PXRD collection, thermal analyses (TGA), <sup>13</sup>C MAS NMR measurements, nitrogen sorption measurements, and SEM micrographs were performed on the technical platforms of IS2M.

## ■ REFERENCES

- (1) Park, K. S.; Ni, Z.; Côte, A. P.; Choi, J. Y.; Huang, R. D.; Uribe-Romo, F. J.; Chae, H. K.; O’Keeffe, M.; Yaghi, O. M. Exceptional Chemical and Thermal Stability of Zeolitic Imidazolate Frameworks. *Proc. Natl. Acad. Sci. U.S.A.* **2006**, *103*, 10186–10191.
- (2) Canivet, J.; Fateeva, A.; Guo, Y.; Coasne, B.; Farrusseng, D. Water Adsorption in MOFs: Fundamentals and Applications. *Chem. Soc. Rev.* **2014**, *43*, 5594–5617.
- (3) Chen, B.; Yang, Z.; Zhu, Y.; Xia, Y. Zeolitic Imidazolate Framework Materials: Recent Progress in Synthesis and Applications. *J. Mater. Chem. A* **2014**, *2*, 16811–16831.
- (4) Duan, J. G.; Jin, W. Q.; Kitagawa, S. Water-Resistant Porous Coordination Polymers for Gas Separation. *Coord. Chem. Rev.* **2017**, *332*, 48–74.
- (5) Phan, A.; Doonan, C. J.; Uribe-Romo, F. J.; Knobler, C. B.; O’Keeffe, M.; Yaghi, O. M. Synthesis, Structure, and Carbon Dioxide Capture Properties of Zeolitic Imidazolate Frameworks. *Acc. Chem. Res.* **2010**, *43*, 58–67.
- (6) Tian, Y.-Q.; Yao, S.-Y.; Gu, D.; Cui, K.-H.; Guo, D.-W.; Zhang, G.; Chen, Z.-X.; Zhao, D.-Y. Cadmium Imidazolate Frameworks with

Polymorphism, High Thermal Stability, and a Large Surface Area. *Chem. - Eur. J.* **2010**, *16*, 1137–1141.

(7) Pimentel, B. R.; Parulkar, A.; Zhou, E.-K.; Brunelli, N. A.; Lively, R. P. Zeolitic Imidazolate Frameworks: Next-Generation Materials for Energy-Efficient Gas Separations. *ChemSusChem* **2014**, *7*, 3202–3240.

(8) Banerjee, R.; Phan, A.; Wang, B.; Knobler, C.; Furukawa, H.; O’Keeffe, M.; Yaghi, O. M. High-Throughput Synthesis of Zeolitic Imidazolate Frameworks and Application to CO<sub>2</sub> Capture. *Science* **2008**, *319*, 939–943.

(9) Zhang, Z.; Zhao, Y.; Gong, Q.; Li, Z.; Li, J. MOFs for CO<sub>2</sub> Capture and Separation from Flue Gas Mixtures: the Effect of Multifunctional Sites on their Adsorption Capacity and Selectivity. *Chem. Commun.* **2013**, *49*, 653–661.

(10) Wang, S.; Wang, X. Imidazolium Ionic Liquids, Imidazolylidene Heterocyclic Carbenes, and Zeolitic Imidazolate Frameworks for CO<sub>2</sub> Capture and Photochemical Reduction. *Angew. Chem., Int. Ed.* **2016**, *55*, 2308–2320.

(11) He, Y.; Zhou, W.; Krishna, R.; Chen, B. Microporous Metal-Organic Frameworks for Storage and Separation of Small Hydrocarbons. *Chem. Commun.* **2012**, *48*, 11813–11831.

(12) Herm, Z. R.; Bloch, E. D.; Long, J. R. Hydrocarbon Separations in Metal-Organic Frameworks. *Chem. Mater.* **2014**, *26*, 323–338.

(13) Qiu, S.; Xue, M.; Zhu, G. Metal-Organic Framework Membranes: from Synthesis to Separation Application. *Chem. Soc. Rev.* **2014**, *43*, 6116–6140.

(14) Van de Voorde, B.; Bueken, B.; Denayer, J.; De Vos, D. Adsorptive Separation on Metal-Organic Frameworks in the Liquid Phase. *Chem. Soc. Rev.* **2014**, *43*, 5766–5788.

(15) Adatoz, E.; Avci, A. K.; Keskin, S. Opportunities and Challenges of MOF-Based Membranes in Gas Separations. *Sep. Purif. Technol.* **2015**, *152*, 207–237.

(16) Bao, Z.; Chang, G.; Xing, H.; Krishna, R.; Ren, Q.; Chen, B. Potential of Microporous Metal-Organic Frameworks for Separation of Hydrocarbon Mixtures. *Energy Environ. Sci.* **2016**, *9*, 3612–3641.

(17) Zhu, Q.-L.; Xu, Q. Metal-Organic Framework Composites. *Chem. Soc. Rev.* **2014**, *43*, 5468–5512.

(18) Bhattacharjee, S.; Jang, M.-S.; Kwon, H.-J.; Ahn, W.-S. Zeolitic Imidazolate Frameworks: Synthesis, Functionalization, and Catalytic/Adsorption Applications. *Catal. Surv. Asia* **2014**, *18*, 101–127.

(19) Dhakshinamoorthy, A.; Opanasenko, M.; Cejka, J.; Garcia, H. Metal Organic Frameworks as Heterogeneous Catalysts for the Production of Fine Chemicals. *Catal. Sci. Technol.* **2013**, *3*, 2509–2540.

(20) Huang, Y.-B.; Liang, J.; Wang, X.-S.; Cao, R. Multifunctional Metal-Organic Framework Catalysts: Synergistic Catalysis and Tandem Reactions. *Chem. Soc. Rev.* **2017**, *46*, 126–157.

(21) Ortiz, G.; Nouali, H.; Marichal, C.; Chaplais, G.; Patarin, J. Energetic Performances of the Metal-Organic Framework ZIF-8 Obtained Using High Pressure Water Intrusion-Extrusion Experiments. *Phys. Chem. Chem. Phys.* **2013**, *15*, 4888–4891.

(22) Ortiz, G.; Nouali, H.; Marichal, C.; Chaplais, G.; Patarin, J. Versatile Energetic Behavior of ZIF-8 upon High Pressure Intrusion-Extrusion of Aqueous Electrolyte Solutions. *J. Phys. Chem. C* **2014**, *118*, 7321–7328.

(23) Ortiz, G.; Nouali, H.; Marichal, C.; Chaplais, G.; Patarin, J. Energetic Performances of “ZIF-71-Aqueous Solution” Systems: A Perfect Shock-Absorber with Water. *J. Phys. Chem. C* **2014**, *118*, 21316–21322.

(24) Ortiz, A. U.; Freitas, A. P.; Boutin, A.; Fuchs, A. H.; Coudert, F.-X. What Makes Zeolitic Imidazolate Frameworks Hydrophobic or Hydrophilic? The Impact of Geometry and Functionalization on Water Adsorption. *Phys. Chem. Chem. Phys.* **2014**, *16*, 9940–9949.

(25) Khay, I.; Chaplais, G.; Nouali, H.; Marichal, C.; Patarin, J. Water Intrusion-Extrusion Experiments in ZIF-8: Impacts of the Shape and Particle Size on The Energetic Performances. *RSC Adv.* **2015**, *5*, 31514–31518.

(26) Khay, I.; Chaplais, G.; Nouali, H.; Ortiz, G.; Marichal, C.; Patarin, J. Assessment of the Energetic Performances of Various ZIFs with SOD or RHO Topology Using High Pressure Water Intrusion-Extrusion Experiments. *Dalton Trans.* **2016**, *45*, 4392–4400.

- (27) Mortada, B.; Chaplais, G.; Veremeienko, V.; Nouali, H.; Marichal, C.; Patarin, J. Energetic Performances of ZIF-8 Derivatives: Impact of the Substitution (Me, Cl or Br) on Imidazolate Linker. *J. Phys. Chem. C* **2018**, *122*, 3846–3855.
- (28) Fraux, G.; Coudert, F.-X.; Boutin, A.; Fuchs, A. H. Forced Intrusion of Water and Aqueous Solutions in Microporous Materials: from Fundamental Thermodynamics to Energy Storage Devices. *Chem. Soc. Rev.* **2017**, *46*, 7421–7437.
- (29) Li, K.; Olson, D. H.; Seidel, J.; Emge, T. J.; Gong, H.; Zeng, H.; Li, J. Zeolitic Imidazolate Frameworks for Kinetic Separation of Propane and Propene. *J. Am. Chem. Soc.* **2009**, *131*, 10368–10369.
- (30) Li, J.; Li, K.; Olson, D. H. Zeolitic Imidazolate Frameworks for Kinetic Separation of Propane and Propene. U.S. Patent US20110282067A1, 2011.
- (31) Groom, C. R.; Bruno, I. J.; Lightfoot, M. P.; Ward, S. C. The Cambridge Structural Database. *Acta Crystallogr., Sect. B: Struct. Sci., Cryst. Eng. Mater.* **2016**, *72*, 171–179.
- (32) Amrouche, H.; Aguado, S.; Pérez-Pellitero, J.; Chizallet, C.; Siperstein, F.; Farrusseng, D.; Bats, N.; Nieto-Draghi, C. Experimental and Computational Study of Functionality Impact on Sodalite-Zeolitic Imidazolate Frameworks for CO<sub>2</sub> Separation. *J. Phys. Chem. C* **2011**, *115*, 16425–16432.
- (33) Hu, J.; Liu, Y.; Liu, J.; Gu, C. Effects of Water Vapor and Trace Gas Impurities in Flue Gas on CO<sub>2</sub> Capture in Zeolitic Imidazolate Frameworks: the Significant Role of Functional Groups. *Fuel* **2017**, *200*, 244–251.
- (34) Amrouche, H.; Creton, B.; Siperstein, F.; Nieto-Draghi, C. Prediction of Thermodynamic Properties of Adsorbed Gases in Zeolitic Imidazolate Frameworks. *RSC Adv.* **2012**, *2*, 6028–6035.
- (35) Moggach, S. A.; Bennett, T. D.; Cheetham, A. K. The Effect of Pressure on ZIF-8: Increasing Pore Size with Pressure and the Formation of a High-Pressure Phase at 1.47 GPa. *Angew. Chem., Int. Ed.* **2009**, *48*, 7087–7089.
- (36) Fairen-Jimenez, D.; Moggach, S. A.; Wharmby, M. T.; Wright, P. A.; Parsons, S.; Düren, T. Opening the Gate: Framework Flexibility in ZIF-8 Explored by Experiments and Simulations. *J. Am. Chem. Soc.* **2011**, *133*, 8900–8902.
- (37) Ania, C. O.; García-Pérez, E.; Haro, M.; Gutiérrez-Sevillano, J. J.; Valdés-Solís, T.; Parra, J. B.; Calero, S. Understanding Gas-Induced Structural Deformation of ZIF-8. *J. Phys. Chem. Lett.* **2012**, *3*, 1159–1164.
- (38) Zhang, C.; Gee, J. A.; Sholl, D. S.; Lively, R. P. Crystal-Size-Dependent Structural Transitions in Nanoporous Crystals: Adsorption-Induced Transitions in ZIF-8. *J. Phys. Chem. C* **2014**, *118*, 20727–20733.
- (39) Tanaka, S.; Fujita, K.; Miyake, Y.; Miyamoto, M.; Hasegawa, Y.; Makino, T.; Van der Perre, S.; Saint Remi, J. C.; Van Assche, T.; Baron, G. V.; et al. Adsorption and Diffusion Phenomena in Crystal Size Engineered ZIF-8 MOF. *J. Phys. Chem. C* **2015**, *119*, 28430–28439.
- (40) Tian, T.; Wharmby, M. T.; Parra, J. B.; Ania, C. O.; Fairen-Jimenez, D. Role of Crystal Size on Swing-Effect and Adsorption Induced Structure Transition of ZIF-8. *Dalton Trans.* **2016**, *45*, 6893–6900.
- (41) Watanabe, S.; Ohsaki, S.; Hanafusa, T.; Takada, K.; Tanaka, H.; Mae, K.; Miyahara, M. T. Synthesis of Zeolitic Imidazolate Framework-8 Particles of Controlled Sizes, Shapes, and Gate Adsorption Characteristics Using a Central Collision-Type Microreactor. *Chem. Eng. J.* **2017**, *313*, 724–733.
- (42) Springuel-Huet, M.-A.; Nossov, A.; Guenneau, F.; Gedeon, A. Flexibility of ZIF-8 Materials Studied Using <sup>129</sup>Xe NMR. *Chem. Commun.* **2013**, *49*, 7403–7405.
- (43) Coudert, F.-X. Molecular Mechanism of Swing Effect in Zeolitic Imidazolate Framework ZIF-8: Continuous Deformation upon Adsorption. *ChemPhysChem* **2017**, *18*, 2732–2738.
- (44) He, M.; Yao, J.; Liu, Q.; Wang, K.; Chen, F.; Wang, H. Facile Synthesis of Zeolitic Imidazolate Framework-8 from a Concentrated Aqueous Solution. *Microporous Mesoporous Mater.* **2014**, *184*, 55–60.
- (45) STOE Powder Diffraction Software Package WinXPOW, version 2.20; STOE & Cie GmbH: Darmstadt, 2006.
- (46) Boulton, A.; Louër, D. Indexing of Powder Diffraction Patterns for Low-Symmetry Lattices by the Successive Dichotomy Method. *J. Appl. Crystallogr.* **1991**, *24*, 987–993.
- (47) Rietveld, H. M. Profile Refinement Method for Nuclear and Magnetic Structures. *J. Appl. Crystallogr.* **1969**, *2*, 65–71.
- (48) Larson, A. C.; Von Dreele, R. B. *General Structure Analysis System (GSAS)*; Los Alamos National Laboratory Report LAUR 86-748, 2004.
- (49) Toby, B. H. EXPGUI, a Graphical User Interface for GSAS. *J. Appl. Crystallogr.* **2001**, *34*, 210–213.
- (50) Le Bail, A.; Duroy, H.; Fourquet, J. L. The Ab-Initio Structure Determination of Lithium Antimony Tungstate (LiSbWO<sub>6</sub>) by X-Ray Powder Diffraction. *Mater. Res. Bull.* **1988**, *23*, 447–452.
- (51) Massiot, D.; Fayon, F.; Capron, M.; King, I.; Le Calvé, S.; Alonso, B.; Durand, J.-O.; Bujoli, B.; Gan, Z.; Hoatson, G. Modelling One- and Two-Dimensional Solid-State NMR Spectra. *Magn. Reson. Chem.* **2002**, *40*, 70–76.
- (52) Rouquerol, J.; Llewellyn, P.; Rouquerol, F. Is the BET Equation Applicable to Microporous Adsorbents? *Stud. Surf. Sci. Catal.* **2007**, *160*, 49–56.
- (53) Walton, K. S.; Snurr, R. Q. Applicability of the BET Method for Determining Surface Areas of Microporous Metal-Organic Frameworks. *J. Am. Chem. Soc.* **2007**, *129*, 8552–8556.
- (54) VandeVondele, J.; Krack, M.; Mohamed, F.; Parrinello, M.; Chassaing, T.; Hutter, J. QUICKSTEP: Fast and Accurate Density Functional Calculations Using a Mixed Gaussian and Plane Waves Approach. *Comput. Phys. Commun.* **2005**, *167*, 103–128.
- (55) Perdew, J. P.; Burke, K.; Ernzerhof, M. Generalized Gradient Approximation Made Simple. *Phys. Rev. Lett.* **1996**, *77*, 3865–3868.
- (56) Grimme, S.; Antony, J.; Ehrlich, S.; Krieg, H. A Consistent and Accurate Ab Initio Parametrization of Density Functional Dispersion Correction (DFT-D) for the 94 Elements H-Pu. *J. Chem. Phys.* **2010**, *132*, No. 154104.
- (57) Bussi, G.; Donadio, D.; Parrinello, M. Canonical Sampling Through Velocity Rescaling. *J. Chem. Phys.* **2007**, *126*, No. 014101.
- (58) Karagiari, O.; Lalonde, M. B.; Bury, W.; Sarjeant, A. A.; Farha, O. K.; Hupp, J. T. Opening ZIF-8: A Catalytically Active Zeolitic Imidazolate Framework of Sodalite Topology with Unsubstituted Linkers. *J. Am. Chem. Soc.* **2012**, *134*, 18790–18796.
- (59) Springer, S.; Baburin, I. A.; Heinemeyer, T.; Schiffmann, J. G.; van Wuelen, L.; Leoni, S.; Wiebcke, M. A Zeolitic Imidazolate Framework with Conformational Variety: Conformational Polymorphs Versus Frameworks with Static Conformational Disorder. *CrystEngComm* **2016**, *18*, 2477–2489.
- (60) Sneddon, S.; Kahr, J.; Orsi, A. F.; Price, D. J.; Dawson, D. M.; Wright, P. A.; Ashbrook, S. E. Investigation of Zeolitic Imidazolate Frameworks Using <sup>13</sup>C and <sup>15</sup>N Solid-State NMR Spectroscopy. *Solid State Nucl. Magn. Reson.* **2017**, *87*, 54–64.
- (61) Cerreia Vioglio, P.; Catalano, L.; Vasylyeva, V.; Nervi, C.; Chierotti, M. R.; Resnati, G.; Gobetto, R.; Metrangolo, P. Natural Abundance <sup>15</sup>N and <sup>13</sup>C Solid-State NMR Chemical Shifts: High Sensitivity Probes of the Halogen Bond Geometry. *Chem. - Eur. J.* **2016**, *22*, 16819–16828.
- (62) Peralta, D.; Chaplais, G.; Paillaud, J.-L.; Simon-Masseron, A.; Barthelet, K.; Pirngruber, G. D. The Separation of Xylene Isomers by ZIF-8: a Demonstration of the Extraordinary Flexibility of the ZIF-8 Framework. *Microporous Mesoporous Mater.* **2013**, *173*, 1–5.
- (63) Pérez-Pellitero, J.; Amrouche, H.; Siperstein, F. R.; Pirngruber, G.; Nieto-Draghi, C.; Chaplais, G.; Simon-Masseron, A.; Bazer-Bachi, D.; Peralta, D.; Bats, N. Adsorption of CO<sub>2</sub>, CH<sub>4</sub>, and N<sub>2</sub> on Zeolitic Imidazolate Frameworks: Experiments and Simulations. *Chem. - Eur. J.* **2010**, *16*, 1560–1571.
- (64) Morris, W.; Doonan, C. J.; Furukawa, H.; Banerjee, R.; Yaghi, O. M. Crystals as Molecules: Postsynthesis Covalent Functionalization of Zeolitic Imidazolate Frameworks. *J. Am. Chem. Soc.* **2008**, *130*, 12626–12627.
- (65) Thompson, J. A.; Blad, C. R.; Brunelli, N. A.; Lydon, M. E.; Lively, R. P.; Jones, C. W.; Nair, S. Hybrid Zeolitic Imidazolate Frameworks: Controlling Framework Porosity and Functionality by Mixed-Linker Synthesis. *Chem. Mater.* **2012**, *24*, 1930–1936.

(66) Xin, Z.; Chen, X.; Wang, Q.; Chen, Q.; Zhang, Q. Nanopolyhedrons and Mesoporous Supra-Structures of Zeolitic Imidazolate Framework with High Adsorption Performance. *Microporous Mesoporous Mater.* **2013**, *169*, 218–221.

(67) Thommes, M.; Kaneko, K.; Neimark, A. V.; Olivier, J. P.; Rodriguez-Reinoso, F.; Rouquerol, J.; Sing, K. S. W. Physisorption of Gases, with Special Reference to the Evaluation of Surface Area and Pore Size Distribution (IUPAC Technical Report). *Pure Appl. Chem.* **2015**, *87*, 1051–1069.

(68) Li, J.-R.; Kuppler, R. J.; Zhou, H.-C. Selective Gas Adsorption and Separation in Metal-Organic Frameworks. *Chem. Soc. Rev.* **2009**, *38*, 1477–1504.

(69) Willems, T. F.; Rycroft, C. H.; Kazi, M.; Meza, J. C.; Haranczyk, M. Algorithms and Tools for High-Throughput Geometry-Based Analysis of Crystalline Porous Materials. *Microporous Mesoporous Mater.* **2012**, *149*, 134–141.

(70) Hobday, C. L.; Bennett, T. D.; Fairen-Jimenez, D.; Graham, A. J.; Morrison, C. A.; Allan, D. R.; Düren, T.; Moggach, S. A. Tuning the Swing Effect by Chemical Functionalization of Zeolitic Imidazolate Frameworks. *J. Am. Chem. Soc.* **2018**, *140*, 382–387.